Atmospheric Compensation of Thermal Infrared Hyperspectral Imagery with the Emissive Empirical Line Method and the In-Scene Atmospheric Compensation Algorithms: A Comparison

Robert J. DiStasio, Jr.[1,2] and Ronald G. Resmini[3]

The MITRE Corporation, 7515 Colshire Drive, McLean, VA, 22102 USA

ABSTRACT

The in-scene atmospheric compensation (ISAC) algorithm of Young et al. (2002) [14] (and as implemented in the ENVI® software system [16] as 'Thermal Atm Correction') is commonly applied to thermal infrared multi- and hyperspectral imagery (MSI and HSI, respectively). ISAC estimates atmospheric transmissivity and upwelling radiance using only the scene data. The ISAC-derived transmissivity and upwelling radiance are compared to those derived from the emissive empirical line method (EELM), another in-scene atmospheric compensation algorithm for thermal infrared MSI and HSI data. EELM is based on the presence of calibration targets (e.g., panels, water pools) captured in the spectral image data for which the emissivity and temperature are well known at the moment of MSI/HSI data acquisition. EELM is similar in concept to the empirical line method (ELM) algorithm commonly applied to visible/near-infrared to shortwave infrared (VNIR/SWIR) spectral imagery and is implemented as a custom ENVI® plug-in application. Both ISAC and EELM are in-scene methods and do not require radiative transfer modeling. ISAC and EELM have been applied to airborne longwave infrared (LWIR; ~7.5 μm to ~13.5 μm) HSI data. Captured in the imagery are calibration panels and/or water pools maintained at different temperatures facilitating the application of EELM. Overall, the atmospheric compensation parameters derived from the two methods are in close agreement: the EELM-derived ground-leaving radiance spectra generally contain fewer residual atmospheric spectral features, although ISAC sometimes produces smoother ground-leaving radiance spectra. Nonetheless, the agreement is viewed as validation of ISAC. ISAC is an effective atmospheric compensation algorithm that is readily available to the remote sensing community in the ENVI® software system. Thus studies such as the present testing and comparing ISAC to other methods are important. The ISAC and EELM algorithms are discussed as are the airborne LWIR and simulated HSI data to which they are applied. Also presented are analyses and comparisons of the retrieved transmissivity and upwelling radiance terms.

Keywords: ISAC, emissive empirical line method, EELM, longwave infrared, LWIR, thermal infrared, hyperspectral, HSI, atmospheric compensation, atmospheric correction, radiance, temperature, emissivity

[1] Send correspondence to Robert DiStasio, The MITRE Corporation, 7515 Colshire Drive, MS T630, McLean, VA, 22102-7508
[2] e-mail: rdistasio@mitre.org, v: 703 983-1428
[3] e-mail: rresmini@mitre.org, v: 703-983-2392

1. INTRODUCTION

1.1. Atmospheric Compensation

Atmospheric compensation is a key processing step for extracting information from thermal infrared (TIR) multi and hyperspectral imagery (MSI and HSI). TIR HSI (and MSI) are impacted by atmospheric transmissivity and additive contributions such as path and reflected downwelling radiance. Atmospheric compensation generates ground-leaving radiance (GLR) data which are then supplied to temperature/emissivity separation (TES) algorithms [9]. The emissivity spectrum is the fundamental datum facilitating material identification and as such, accurate and robust atmospheric compensation is required for the generation of high-quality spectral signatures.

Here, we present a comparison of two atmospheric compensation algorithms. Both are in-scene techniques (in contrast to radiative transfer (RT) and hybrid RT/in-scene methods; e.g., [1, 4]); one method is readily available to the user community in the ENVI® software system; the other is implemented as a custom ENVI® plug-in. Algorithm performance is assessed by comparisons of the retrieved atmospheric transmissivity and additive terms as well as an examination of retrieved emissivity spectra.

1.2. Current Methods

There are two main approaches to atmospheric compensation of TIR spectral image data, in general, and of LWIR HSI in particular.

1.2.1. Radiative Transfer (RT) Modeling

In this method the atmospheric column is modeled as exactly as possible using the radiative transfer equation often tuned with known atmospheric conditions. A benefit of this method is not requiring a priori knowledge of in scene objects and materials and the ability to apply the technique to data acquired at any geographic location. The main difficulty with RT modeling is being able to exactly model the atmospheric column corresponding to that of the data set, which generally entails multiple runs of the RT code (e.g. MODTRAN [17]). Additionally any model contains built-in assumptions that will generate approximate results which may or may not have an impact on the resulting atmospherically corrected ground-leaving radiance data cube.

1.2.2. In-Scene

In-scene atmospheric correction methods use the actual remotely-sensed at-aperture radiance data in the hyperspectral image cube to compensate for the atmosphere, thus allowing the user to utilize the exact state of the atmosphere. The main advantage of in-scene methods over model-based methods is that they capture the true state of the atmosphere (and the complicated radiative processes occurring therein) at the time of data collection. The main difficulty for in-scene methods is identifying and estimating correctly the input parameters for the correction algorithm.

1.3. Objective

This paper presents a comparison of two in-scene atmospheric correction methods: the Emissive Empirical Line Method (EELM) and the In-Scene Atmospheric Correction (ISAC) algorithms for the LWIR (~7.5 μm to ~13.5 μm) portion of the spectrum. EELM and ISAC were applied to airborne HSI LWIR data sets and the common parameters generated were compared: atmospheric transmission,τ, upwelling radiance, L_u, and the resulting ground-leaving radiance (GLR) spectra of the corrected data cubes. Data were processed using the ENVI® (Environment for Visualizing Images) software [16].

2. PROCESS

2.1. Atmospheric Correction Methods

2.1.1. EELM

The Emissive Empirical Line Method (EELM) is the infrared extension of the Empirical Line Method (ELM) atmospheric correction. EELM employs a linear regression for each band to equate at-sensor radiance to ground leaving radiance (GLR) via target emissivity and temperature by generating atmospheric transmission, upwelling radiance, and downwelling radiance terms. EELM requires at least three sets of values of at-sensor radiance from the HSI cube, their corresponding emissivity spectra (from ground truth and/or library), and temperature. Outputs include the generation of atmospheric profile plots as well as the generation of a GLR data cube that may be used as an input to a temperature emissivity separation (TES) algorithm.

EELM was implemented with a custom ENVI® plug-in routine[4]. The code matches emissivity and HSI data cube spectra, which is normally accomplished by creating regions of interest (ROI) on calibration targets in the imagery and pairing the ROIs with library or in-situ measured emissivity spectra and material temperature.

2.1.2. ISAC

The In-Scene Atmospheric Correction (ISAC) algorithm is described in Young et al., (2002); see also refs. [6,7,10,14,15]. ISAC requires only the calibrated, at-aperture radiance data to estimate the upwelling radiance and transmissivity of the atmosphere by solving equation (1) which is derived from the general RT expression for at-aperture radiance and with the assumption that objects with the highest radiance are blackbodies or blackbody-like.

$$L_{obs} = \tau B(T) + L_u \quad (1)$$

In eq. (1), L_{obs} is the observed, at-aperture radiance, τ is the transmission of the atmosphere, B(T) is the Planck function, and L_u is the upwelling radiance due to the atmosphere.

ISAC estimates the ground leaving radiance from the brightness temperature of each pixel. Then, for each band, a scatter plot is produced between the observed radiance and the Planck function. A straight line is fit to the top of the scatter plot. The top of the plot corresponds to those pixels whose emissivity is closest to 1.0. From this fit, the transmission (slope) and upwelling radiance (intercept) are estimated. The transmission and upwelling terms are then used to estimate the ground leaving radiance from at sensor radiance for each pixel in the original HSI cube.

Outputs include the generation of atmospheric profile plots of transmission and upwelling (τ, L_u) as well as the generation of a GLR data cube that can be used as an input into a TES algorithm.

In ENVI®, a version of ISAC is implemented as 'Thermal Atm Correction'.

2.2. Data Sets

Two separate data sets were utilized in this study.

2.2.1. SEBASS Experimental Data Set

The Spatially Enhanced Broadband Array Spectrograph System (SEBASS) is an airborne hyperspectral imaging spectrometer designed and built by the Aerospace Corporation [4,6] that collects in the mid- and longwave infrared regions of the spectrum. In the LWIR, 128 contiguous spectral bands are measured simultaneously in the along-track direction for 128 cross track pixels. The instantaneous field of view of the fore-optics is 1.1 mrad per pixel with a total field of view of 128 mrad. Additional sensor details and example applications may be found in refs. [8, 11, 12,13]. SEBASS midwave infrared (MWIR) data was not utilized.

SEBASS LWIR HSI data were collected over an area containing water pools maintained at three different temperatures. The SEBASS data analyzed here were acquired in July 2005, at 12:33:42 GMT at an altitude of ~1667 feet above ground level (AGL) and thus have a ground sample distance (GSD) of ~22 inches. The SEBASS Experimental Data Set is distinct in time and location from the data set to be described next.

[4] The EELM module was created by Dave Miller of the former Spectral Information Technology Application Center (SITAC).

2.2.2. SHARP Data

The SEBASS High Altitude Research Project (SHARP) is the high altitude variant of the SEBASS system. SHARP is operated from a WB-57F aircraft and designed to work at high altitude. The sensor collected data on 20 May 2003, at nominal altitudes of 20 and 50 Kft AGL for both nadir and 70^{o} off-nadir data over a target area at Ellington Airfield in Houston, TX. However, only the nadir data was utilized for this study. Nine flight lines were acquired over the target array area, with six in nadir configuration (four at 20 Kft AGL and two at 50 Kft AGL), each flight line containing 1-5 data sets, depending on weather and viewing geometries.

2.3. Ground-Truth Data

2.3.1. Water Pools in the SEBASS Experimental Data Set

A chip of the SEBASS data and a false-color composite high-resolution context image corresponding to the area of coverage are shown in Figure 1. The low, medium, and high temperature pools are indicated by the dark, medium, and light grayscales, respectively, in the SEBASS image chip. Each water pool contains at least a dozen SEBASS pixels available for the application of EELM that are away from the pools' edges.

Figure 1: (left) A 10.73 μm grayscale image chip of SEBASS LWIR HSI data showing three water pools. (right) A false-color composite high-resolution context image corresponding to the area in the SEBASS image on the left. The water pools are the three green circular features

2.3.2. Ellington Field, Houston, Texas

Sixteen targets were deployed on a low grassy field ~ ½ mile from the WB-57F hangar at Ellington Field. Target materials and their relative deployment positions are given in Figure 2. Ten targets were instrumented with contact thermocouples (Omega Engineering #SA1-T) placed on opposite corners of the panels. Three infrared thermocouples (Omega Engineering #OS-36-T) were placed to measure water pool temperature, while a fourth was placed to measure the sand pit. One end of the water pool was constructed several inches higher than the other, causing the pool to overflow the low end, so only ~ 2/3 of water-containing pool pixels are available in the imagery for analysis. Several specialty targets were not utilized for this effort: Tyvek striped target, ice pool, aluminum tarp and a point source. Multiple spectral measurements were undertaken using a Designs & Prototypes (D&P) fourier transform spectrometer, model 102F, with a resolution of ~ 4cm^{-1} [3].

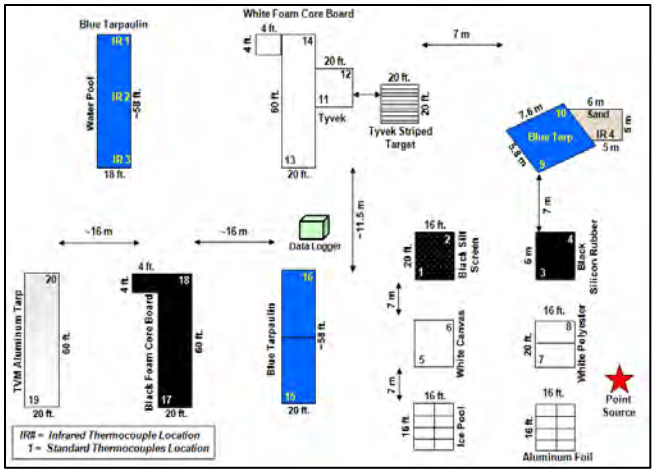

Figure 2: Ellington Field target material array.

2.4. METHODS

2.4.1. SEBASS Experimental Data Set

ENVI®'s Thermal Atm Correction was applied to a spatial subset of the data (not shown in Figure 1) adjacent to the water pool area and containing only vegetation. The atmospheric parameters obtained were then applied to the entire scene, with each pixel in the data set divided by the transmissivity after subtraction of the upwelling radiance term.

EELM was applied twice to the data using the aforementioned ENVI® Plug-In. First, water pool temperatures were derived from processing the SEBASS data with ENVI®'s Thermal Atm Correction to obtain ground-leaving radiance (GLR), followed by the normalized emissivity method (NEM) [5] temperature emissivity separation (TES) technique (implemented in ENVI® as Emissivity Normalization). These temperatures (299.0, 302.6 and 308.6 K) were then used in EELM with an ideal flat LWIR emissivity (ε) spectrum for water with a value of 0.99. The second application of EELM used the same temperatures with a laboratory-measured distilled water reflectance spectrum converted to emissivity using Kirchhoff's Law.

Water bath temperatures were also estimated from a single band of at-aperture radiance values at which ε is at or above 0.99 (actually 0.997) and L_u is very low (0.20 μflicks) as determined by an application of ENVI®'s Thermal Atm Correction. For this SEBASS data set, this corresponded to the 9.24 μm band. The temperatures obtained were identical to those obtained by the Thermal Atm Correction/NEM method.

The water pools were also instrumented with thermocouples. However, temperatures derived from them (and coincident with the data collection) were spurious and generated unrealistic EELM atmospheric parameters.

2.4.2. Ellington Field

Each flight line was evaluated and the individual images reviewed for cloud cover, data quality, and to determine if the entire target array was captured in the imagery. The best image cubes for low and high altitude that contained the entire target array were identified for processing. ENVI® Thermal Atm Correction was run on these selected cubes, using a normalized regression fitting technique (SHARP NESR ~0.46).
For EELM, regions of interest (ROI) were created over the center of several targets that were to be used for calibration. Targets selected for nadir data were aluminum foil, water pool, black foam core, silt screen, and Tyvek. For the high altitude passes, Tyvek was not utilized due to its close proximity to the white foam core target, which could cause mixing due to adjacency. ENVI® spectral libraries of target emissivities were created from ground-truth spectral measurements and resampled to SHARP band-center wavelengths and band shapes. Temperatures were initially taken from thermocouple measurements. However, the variability between the two thermocouples placed on the panels was large and in at least one case a thermocouple became detached from the target. For some targets, differences were reasonable, but in a number of cases they disagreed by several degrees with the extreme being Tyvek where the mean temperature difference was over 8°C. It can be shown with modeled data that EELM is very sensitive to target temperature and so an alternative method for estimating temperature was sought and utilized.
Target material temperature may be estimated directly from the radiance data. First, assume that there is a band for which the atmospheric transmissivity is ~100% and for which the downwelling radiance term is ~0 (and, ideally, the material is blackbody-like at that band). The band at ~9.24 μm meets these criteria. Applying the calculation given in Appendix A, radiance equation is solved for the temperature (in K). For the SHARP sensor, this gives:

$$T = (-1558.5330)/((LN(L_{Observed}) - LN(\epsilon) - 12.0870)) \quad (2)$$

The temperature for the targets was calculated using the mean radiance over the ROI of the target and with the emissivity of the target at 9.24 μm , generating a temperature based on equation 2. This temperature estimate, the emissivity spectra, and the ROI's were input to EELM. Outputs, including plots of τ and L_u, were generated and compared EELM results were also compared to those from ISAC.

3. RESULTS

3.1. Atmospheric Parameters

3.1.1. SEBASS Experimental Data Set

Figure 3 shows a comparison of the τ and L_u terms obtained from EELM (with the ideal, flat emissivity spectrum of water) and Thermal Atm Correction (indicated as ISAC in the figure). The agreement in both plots is very good particularly with respect to the location of the atmospheric absorption features and their shapes. There is, however, a slight difference in magnitude evident in both plots. This is perhaps due to Thermal Atm Correction being applied to a portion of the scene containing real vegetation (with ε = ~0.98) compared to EELM applied with an ideal water emissivity spectrum with a value of 0.99. Similar results are obtained in the comparison of EELM applied with the real distilled water emissivity spectrum and Thermal Atm Correction; the τ and L_u terms are in very good agreement.

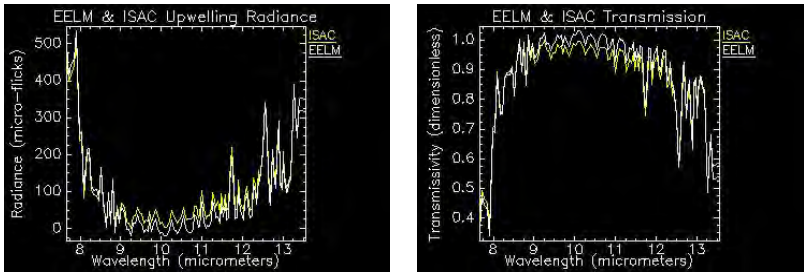

Figure 3: Comparison of the τ and L_u terms obtained from EELM applied with the ideal, flat water emissivity spectrum and from ENVI®'s Thermal Atm Correction. [5]

3.1.2.Ellington Field

3.1.2.1. Atmospheric Conditions

The atmosphere at Ellington Field is generally humid and aerosol laden, given its proximity to the Gulf Coast industrial city of Houston, Texas. Houston's proximity to a very moist maritime atmosphere further complicates the atmospheric column.

3.1.2.2. ISAC

ISAC was applied to several SHARP images, and in the following figures the resulting atmospheric profiles are shown along with the resulting radiance spectra over a grass pixel. Note the noise below 8 μm and above 13 μm in the radiance spectra. This behavior is consistent across all data sets regardless of the manner of atmospheric correction.

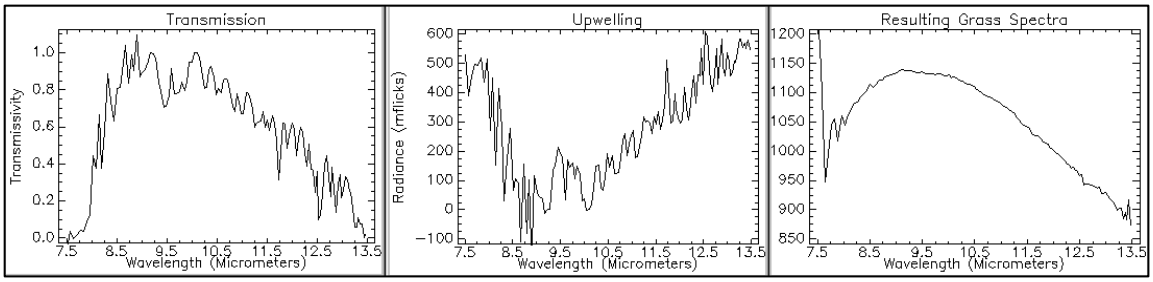

Figure 4: Low-altitude ISAC Results.

[5] A μflick is a unit of radiance in: $\mu W/cm^2.sr.\mu m$.

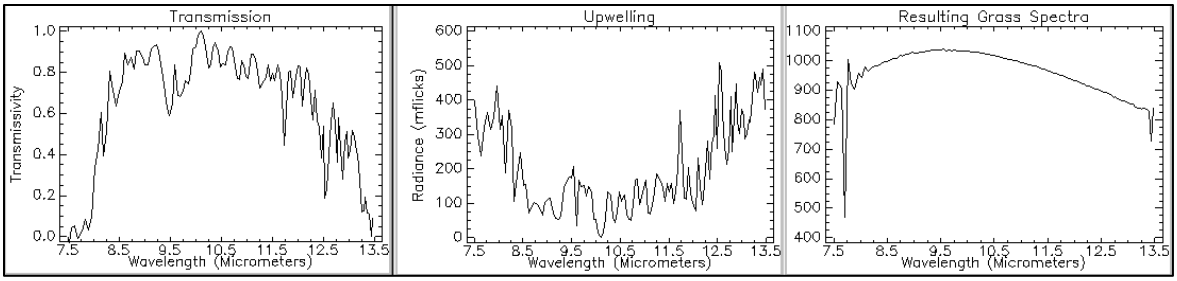

Figure 5: High-Altitude ISAC Results.

3.1.2.3. EELM

After multiple applications of EELM, it was found that the use of three panels produced the best atmospheric correction. Adding additional calibration panels only marginally improved and sometimes degraded performance. Figures 6-9 present the best EELM results.

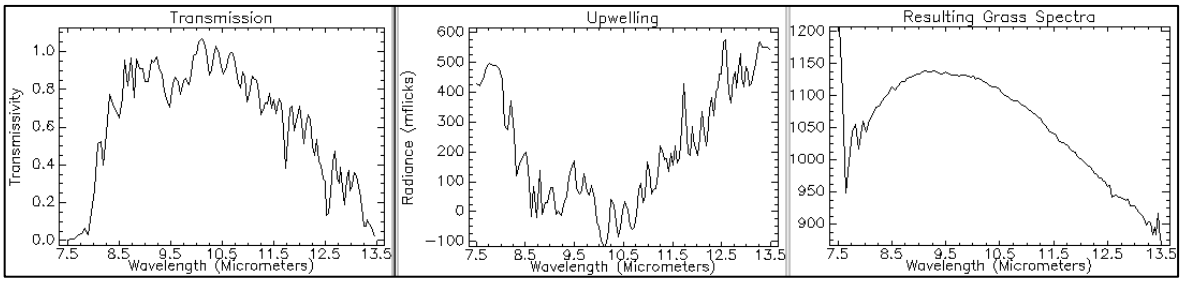

Figure 6: Low-altitude EELM Results

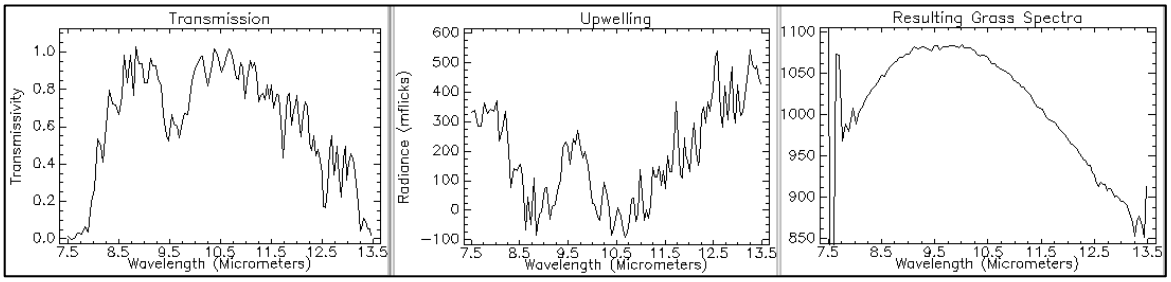

Figure 7: Low-altitude EELM Results

3.1.2.4. Comparison

Atmospheric parameter comparison at Ellington was variable, showing distinct differences between the two methods.

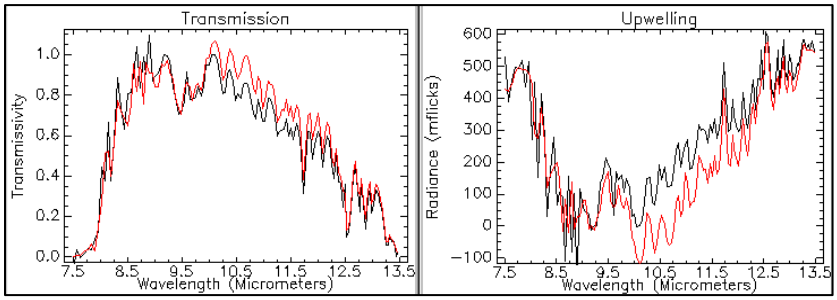

Figure 8: Nadir-looking atmospheric terms: τ (left) and L_u (right). ISAC results are in black, EELM in red.

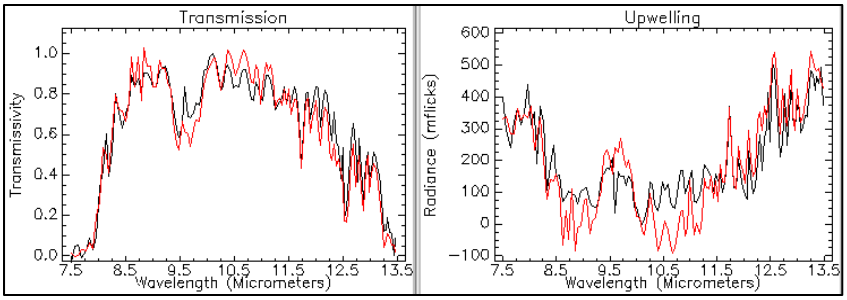

Figure 9: High-altitude, nadir-looking atmospheric terms: τ (left) and L_u (right). ISAC results are in black, EELM in red.

3.2. Spectra Comparison

3.2.1. SEBASS Experimental Data Set

Figure 10 shows two ground-leaving radiance (GLR) spectra of a pixel of concrete in the region near the water pools derived from applying EELM (with the flat ε water spectrum) and Thermal Atm Correction (ISAC). Though the two spectra are in very good agreement, the EELM GLR spectrum has less residual atmospheric features particularly in the 7 to 9 micrometer range. Figure 11 shows a GLR spectrum of a single vegetation pixel near the water pools and a plot of the best-fit Planck function for comparison. The two plots are in remarkable agreement.

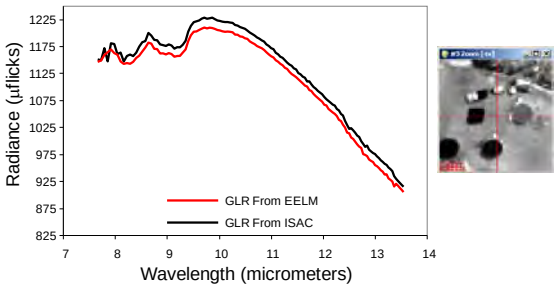

Figure 10: Ground-leaving radiance (GLR) from EELM (red) and ISAC (black).

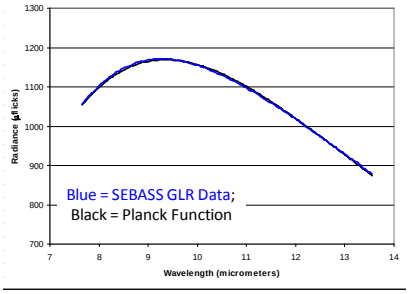

Figure 11: Ground-Leaving Radiance (GLR) from EELM for a single vegetation pixel.

Figure 12 shows two emissivity spectra of the same pixel of concrete discussed above, obtained by applying the NEM TES to the GLR spectra. Once again, the spectra are in very good agreement; however, the EELM/NEM spectrum has fewer residual atmospheric features in the 7 to 9 μm range.

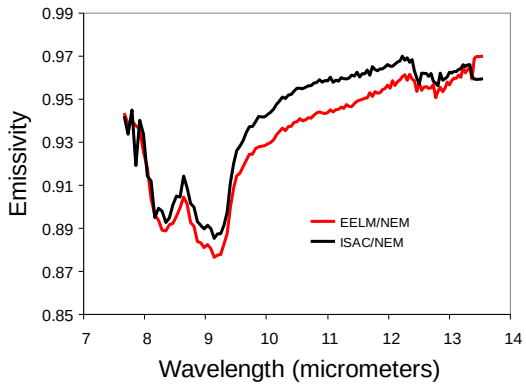

Figure 12: Emissivity Spectra from EELM/NEM (red) and ISAC/NEM (black).

3.2.2. Ellington field

Figure 13 shows the comparison between the GLR from both ISAC results are in black, EELM in red. While noisy below 8 μm and above 12.5 μm, the spectral curves are generally well behaved, with ISAC generally smoother than EELM.

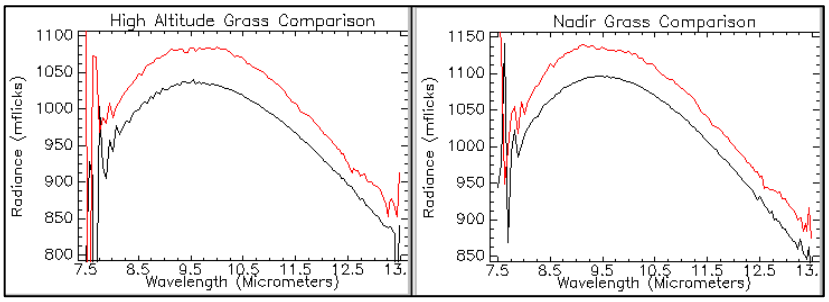

Figure 13: Ground Leaving Radiance comparison. ISAC (red) and EELM (yellow).

As a final test, NEM was run on the ISAC and EELM GLR spectra. In Figure 14 the emissivity spectra of several pixels are plotted for sand and White Foam Core and compared to the ground truth measurements (in green and blue). While differing in details, the pixels from both NEM results appear to match the major features of the ground targets, although not in magnitude. It is interesting that both ISAC and EELM-derived emissivity spectra match much closer to damp sand rather than dry sand.

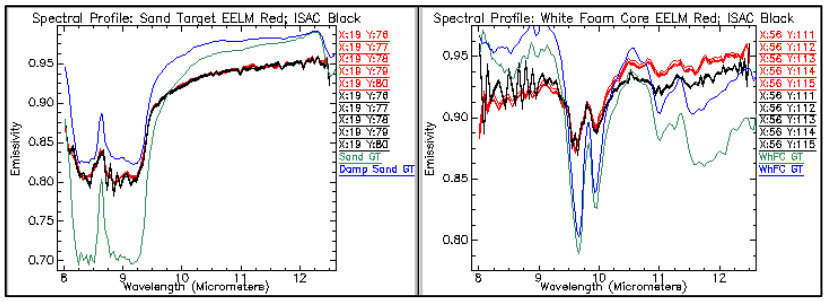

Figure 14: Emissivity spectra comparison. Emissivity is derived from applying the normalized emissivity method (NEM) temperature/emissivity separation (TES) algorithm.

4. ANALYSIS AND DISCUSSION

The data sets analyzed in this study facilitate a comparison of atmospheric correction algorithm performance in atmospheres of different complexity in terms of turbidity, humidity, and column (or path) length. For the SHARP Ellington Field and SEBASS Experimental Data Sets, the τ and L_u atmospheric terms derived from EELM and ISAC were in good agreement. In the SEBASS Experimental Data Set the terms are practically identical and even in the more complex Ellington Field atmosphere the τ and L_u terms are similar in many respects. Both ISAC (implemented as Thermal Atm Correction in ENVI®) and EELM generated accurate GLR spectra (in terms of a comparison to the Planck function), and when subsequently processed with NEM, the resulting emissivity signatures are in good agreement with ground-truth data. These results indicate that in-scene methods for LWIR atmospheric compensation are robust. Further, the results obtained here are viewed as a validation of ISAC (as implemented in ENVI®). Because of the availability of ENVI, the remote sensing user community has access to an effective, easy to use, atmospheric compensation tool for LWIR HSI (and MSI) data.

There is one potential limiting factor for using an in-scene method such as EELM (or ISAC) applied to a spatial subset of a larger HSI data set). Strictly speaking, the atmospheric compensation terms (i.e., τ and L_u) are applicable only to the atmospheric column from which they were derived. The coefficients are, however, generally applied to an entire HSI data set (this issue applies as well to ELM for VNIR/SWIR HSI). I.e., it is generally not known a priori how far away from the EELM calibration targets one can stray before the atmospheric parameters no longer apply. Stated alternatively, the horizontal variability of the atmosphere over an HSI data set of arbitrary size is generally not known prior to data analysis. Both data sets in this study are small in areal extent, on the order of a few kilometers at most, and so atmospheric variation is assumed to be minimal. Further study utilizing larger sized data sets is recommended in order to determine the range of applicability of a given set of in-scene derived atmospheric compensation terms.

Additional areas for future work include the application of in-scene methods to LWIR (and MWIR) data acquired at night and to off-nadir data.

5. SUMMARY AND CONCLUSIONS

We presented herein the results of a comparison of two in-scene atmospheric compensation methods for thermal infrared spectral image data: EELM and ISAC (as Thermal Atm Correction in ENVI®). The data sets to which the algorithms were applied differed in their atmospheric conditions. For a given data set, ISAC and EELM produced very similar GLR spectra displaying only minor differences in detail (e.g., residual atmospheric absorption features) and magnitude. These results, when subsequently processed with a temperature/emissivity separation algorithm, generated emissivity spectra that closely matched ground-truth spectra in terms of general shape and locations of major absorption features.

Even though relatively good GLR spectra are obtained, the atmospheric terms (τ and L_u) produced by EELM and ISAC sometimes differed and the differences were, in some cases, non-trivial, although major atmospheric features are generally matched. It was also noted that the resulting GLR spectra had anomalies above 13 μm and below 8μm, especially for the Ellington Field data. However, these variations did not preclude the generation of relatively good GLR spectra throughout most of the LWIR atmospheric window spectral range.

EELM is an effective LWIR atmospheric compensation algorithm that produces GLR spectra that compare favorably to the Planck function. This is perhaps expected because the method is an extension of ELM, which has been shown to be the most effective atmospheric correction algorithm for VNIR/SWIR HSI data. However, the method is very sensitive to temperature and, to a lesser extent, the emissivity signature of the required in-scene target materials. Temperature variability was an issue in this study as ground measurements displayed unacceptable, large variability; accurate temperature measurements are required for the successful application of EELM—though those estimates may be derived from the data themselves with the careful application of various techniques for infrared temperature measurement. ISAC, as provided in ENVI®, is also highly effective for atmospheric correction. The very close agreement between the ISAC and EELM τ and L_u terms is viewed as a validation of ISAC (as provided in ENVI) for use with LWIR imagery.

The results presented here confirm the robustness of two in-scene atmospheric compensation methods for LWIR spectral image data. Remote sensing practitioners may use these methods with confidence for their processing and analysis of TIR spectral image data.

APPENDIX A. FINDING TEMPERATURE BASED ON THE LWIR RADIANCE.

Start with Radiance equation:

$$L = [\epsilon B(\lambda, T) + (1 - \epsilon)L_{DN}]\tau + L_{UP} \quad \text{(A-1)}$$

Where L is the target radiance, ϵ *is the target emissivity*, $B(\lambda, T)$, is the blackbody Planck function ($\boldsymbol{C_1}/\{\boldsymbol{\lambda^5}\left[\boldsymbol{e^{\frac{c_2}{\lambda T}} - 1}\right]$), τ is the atmospheric transmission, L_{UP} is the upwelling radiance and L_{DN} is the downwelling radiance.

Combining for the sensor observed radiance:

$$L - L_{UP} = L_{Observed} = [\epsilon B(\lambda, T) + (1 - \epsilon)L_{DN}]\tau \quad \text{(A-2)}$$

Assumption 1: Work at a wavelength where the transmission $\tau \approx 1$

{This occurs at a wavelength of 9.24μmor for the Sharp sensor in band30 (Band Center of 9.2324μ) for SHARP}

$$L(\lambda) = [\epsilon B(\lambda, T) + (1 - \epsilon)L_{DN}] \quad \text{(A-3)}$$

Assumption 2: Term $(1 - \epsilon)L_{DN}$ is negligible and can be safely ignored for your material.

Then

$$L_{Observed} \cong [\epsilon B(\lambda, T)] \quad \textbf{Or} \quad \textbf{(A-4)}$$

$$\frac{L}{\epsilon} = \boldsymbol{B(\lambda, T) = C_1/\{\lambda^5\left[e^{\frac{c_2}{\lambda T}} - 1\right]\}} \quad \textbf{(A-5)}$$

Taking the natural log of both sides...

$$LN(L_{OBS}) - LN\ (\epsilon) = LN(C1) - 5 * LN(\lambda) - \frac{C2}{\lambda T} + LN\ (1) \quad \text{(A-6)}$$

Substituting values for SHARP, including wavelength $\lambda = 9.2324\ microns$:
(Note: Constants have units appropriate for SHARP (e.g., micro flicks) sensor)

$$LN(L_{OBS}) - LN\ (\epsilon) = LN(1.191^{-10}) - 5 * LN(0.00092324) - \frac{1.4389}{0.00092324T} + 0$$

$$LN(L_{OBS}) - LN\ (\epsilon) = -22.8511 - (5 * -6.9876) - \frac{1.4389}{0.00092324T}$$

$$LN(L_{OBS}) - LN\ (\epsilon) = 12.0870 - \frac{1558.5330}{T}$$

Solving for T:

$$\boldsymbol{T = \frac{-1558.5330}{(LN(L_{Observed}) - LN\ (\epsilon) - 12.0870)}} \quad \textbf{(A-7)}$$

So now one can estimate temperature in degrees Kelvin using observed target radiance from SHARP band 30 and the target emissivity at 9.2324 μm.

ACKNOWLEDGMENTS

The HSI data were provided by the Basic and Applied Research Office (IB) of the Innovision Directorate of the National Geospatial-Intelligence Agency (NGA), Reston, VA, U.S.A.

REFERENCES

1. Boonmee, M., Schott, J.R., and Messinger, D.M., (2006). Land surface temperature and emissivity retrieval from thermal infrared hyperspectral imagery. In: Proceedings of the SPIE, Algorithms and Technologies for Multispectral, Hyperspectral, and Ultraspectral Imagery XII, S.S. Shen and P.E. Lewis, eds., v. 6233, doi: 10.1117/12.665899, Orlando, Fla., 17-21 April, 11 p.
2. Borel, C., (2008). Error analysis for a temperature and emissivity retrieval algorithm for hyperspectral imaging data. International Journal of Remote Sensing, v. 29, nos. 17-18, doi:10.1080/01431160802036540, pp. 5029-5045.
3. D&P Industries; *MODEL 102 PORTABLE FTIR INSTRUCTION MANUAL Version 1.2* Simsbury, CT May 2006. http://www.dpinstruments.com/papers/102_W2K_Instruction_Manual_v1_2_with_pic.pdf
4. Gillespie, A. R. (1985). Lithologic mapping of silicate rocks using TIMS. The TIMS Data User's Workshop. JPL Publication 86-38, Jet Propulsion Laboratory, Pasadena, CA, pp. 29-44.
5. Gruninger, J., Fox, M., Lee, J., Ratkowski, A.J., and Hoke, M.L., (2002). Use of Vis-SWIR to aid atmospheric correction of multispectral and hyperspectral thermal infrared (TIR) imagery: the TIR model. In: Proceedings of the SPIE, Imaging Spectroscopy VIII, v. 4816-11, July, 2002, 13 p.
6. Hackwell, J. A., Warren, D. W., Bongiovi, R. P., Hansel, S. J., Hayhurst, T. L., Mabry, D. J., Sivjee, M. G., & Skinner, J. W. (1996). LWIR/ MWIR Imaging Hyperspectral Sensor for Airborne and Ground-Based Remote Sensing. *SPIE, 2819, 102– 107*.
7. Kaiser, R., Vititoe, D., and Andrews, A., (2003). Detecting low-emissivity objects in LWIR hyperspectral data and the corresponding impact on atmospheric compensation. In: Proceedings of the SPIE, Algorithms and Technologies for Multispectral, Hyperspectral, and Ultraspectral Imagery IX, S.S. Shen and P.E. Lewis, eds., Orlando, Fla., April 21-25, v. 5093, pp. 705-718.
8. Kirkland, L. E., K. C. Herr, E. R. Keim, P. M. Adams, J. W. Salisbury, J. A. Hackwell, A. Treiman, (2002). First Use of an Airborne Thermal Infrared Hyperspectral Scanner for Compositional Mapping. Remote Sensing of Environment, v. 80, pp. 447-459.
9. McCabe, M.F., Balick, L.K., Theiler, J., Gillespie, A.R., and Mushkin, A., (2008). Linear mixing in thermal infrared temperature retrieval. International Journal of Remote Sensing, v. 29, nos. 17-18, doi:10.1080/01431160802036474, pp. 5047-5061.
10. Pascucci, S., Bassani, C., Palombo, A., Poscolieri, M., and Cavalli, R., (2008). Road asphalt pavements analyzed by airborne thermal remote sensing: preliminary results of the Venice Highway. Sensors, v. 8, ISSN 1424-8220, pp. 1278-1296.
11. Vaughan, R.G., Hook, S.J., Calvin, W.M., and Taranik, J.V., (2005). Surface mineral mapping at Steamboat Springs, Nevada, USA, with multi-wavelength thermal infrared images. Remote Sensing of Environment, v. 99, doi:10.1016/j.rse.2005.04.030, pp. 140-258.
12. Vaughan, R.G., Hook, S.J., Calvin, W.M., and Taranik, J.V., (2003). SEBASS Hyperspectral Thermal Infrared Data: Surface Emissivity Measurement and Mineral Mapping. Remote Sensing of Environment 85 (2003) 48–63
13. Vaughan, R.G., and Calvin, W.M., (2004). Synthesis of high-spatial resolution hyperspectral VNIR/SWIR and TIR image data for mapping weathering and alteration minerals in Virginia City, Nevada. In: Proceedings of the International Geoscience and Remote Sensing Symposium (IGARSS '04), v. 2, pp. 1296-1299, doi: 10.1109/IGARSS.2004.1368654, 20-24 Sept., 2004.
14. Young, S.J., Johnson, R.B., and Hackwell, J.A., (2002). An in-scene method for atmospheric compensation of thermal hyperspectral data. Journal of Geophysical Research, v. 107, no. D24, 4774, doi:10.1029/2001JD001266, 20 p.
15. Young, S. J. (1998). In scene atmospheric compensation: Application to SEBASS data collected at the ARM Site. Part II. *Aerospace Corporation technical report*, ATR-99 (8407)-1.
16. http://www.ittvis.com/envi/ .
17. http://www.modtran.org/ .